J Mater Sci (2010) 45:5045–5053
DOI 10.1007/s10853-010-4334-6

ICAM 2009

Electronic states in double quantum well-wires with potential W-profile: combined effects of hydrostatic pressure and electric field

R. L. Restrepo · G. L. Miranda · C. A. Duque

Received: 30 November 2009 / Accepted: 18 February 2010 / Published online: 6 March 2010

Abstract Within the framework of the effective mass and parabolic band approximations and using a variational procedure, a detailed theoretical study of the combined effects of hydrostatic pressure and in-growth direction applied electric field on the electronic states and binding energy of a donor impurity in a GaAs–(Ga,Al)As coupled double quantum well-wires is presented. The particular situation of W-shaped confining potential profile is analyzed. The results obtained show that the energy for the first confined electron states as well as the impurity binding energy bear strong dependences with the hydrostatic pressure, the strength of the applied electric field, and the shape of the confining potential barriers. In the case of the electron states, it is observed that their energies are increasing (decreasing) functions of the potential-shape-related Λ-parameter (hydrostatic pressure). It is also found that, in the high hydrostatic pressure regime (25 kbar in this work), the binding energy of a donor impurity decreases with the pressure and the effects of hydrostatic pressure on the potential barriers are predominant over the effects of hydrostatic pressure on the GaAs static dielectric constant. It is shown that the binding energy can increase or decrease depending on the combined effects of the applied electric field and the dimensions of the transversal section of the coupled quantum well wires.

R. L. Restrepo (✉) · G. L. Miranda
Física Teórica y Aplicada, Escuela de Ingeniería de Antioquia,
A.A. 7516 Medellin, Colombia
e-mail: pfrire@eia.edu.co

R. L. Restrepo · G. L. Miranda · C. A. Duque
Instituto de Física, Universidad de Antioquia,
A.A. 1226 Medellin, Colombia

Introduction

The advances in experimental crystal-growth techniques have revealed new opportunities to study the optoelectronic properties and band structure of semiconductor superlattices and heterostructures. The set of different alternatives by which it is possible to manipulate such nanodevices is called the engineering of the quantum confinement. Among these systems, potential W-profile quantum well-wires have attracted considerable interest due to the occurrence of new physical phenomena as well as their possible applications in photo-detectors and other optoelectronic devices [1–19].

Many theoretical investigations have calculated the first few hydrogenic impurity states, the binding energies, and the impurity related optical properties associated with shallow-donor and/or shallow-acceptor impurities in low-dimensional systems such us quantum wells (QW), quantum-well wires (QWW), and quantum dots (QD). Some works deal with the effects of hydrostatic pressure on exciton and shallow-donor impurity states in single GaAs–$Ga_{1-x}Al_xAs$ QW [1–3], single GaAs–$Ga_{1-x}Al_xAs$ QWW [4, 5], and isolated QD [6]. All these works have considered abrupt potential barriers which confine the carriers into the region on the quantum system. Using a variational procedure within the effective-mass and parabolic band approximations, the simultaneous effects of temperature, hydrostatic pressure and applied electric and magnetic fields on shallow-donor impurity states in single square QW and double square QWW have been also reported [7–9].

The combined hydrostatic pressure and applied electric field effects on the donor-impurity states in double-coupled QW with square and triangular well potentials have been reported by Raigoza et al. [20] and Kasapoglu et al. [10].

They found that associated with the breaking of the symmetry—as effect of the applied electric field—the density of impurity states is richer in structures. Also, they claim that depending on the impurity position along the growth direction of the structure, the impurity binding energy is an increasing and/or decreasing function of the applied electric field. The mixing of square and triangular well potentials has been considered in the study of the electron-energy spectrum and of the binding energy of a shallow-donor impurity confined in single GaAs–(Ga,Al)As rectangular-transversal section QWWs [11–13]. As a general trend they found that: (1) due to the two-dimensional confinement, the binding energy in one-dimensional-systems is approximately twice the binding energy in single QW, and (2) the binding energy of donor impurities strongly depends on the external inputs such as the pressure and the applied electric field, and also on the structural features of the low dimensional system.

The Intense laser effects and the nonparabolicity on the electronic and donor states in QW with V- and W-shape confinement potential have been studied by Niculescu et al. [14] and Vanitha and Peter [15]. They found that the binding energy depends sensitively on the geometric confinement and the impurity position. Low-dimensional heterostructures with W-profile confinement potential present a higher nonlinear optical rectification than the single and coupled square quantum wells, which has significant influences on improvements of optical devices, such us, ultrafast optical switches, infrared waveguide devices and so on [16–19].

Stimulated by the works of Bilekkaya et al. [12], Aktaş et al. [13], Niculescu et al. [14], Vanitha and Peter [15], the present work is concerned with a theoretical study of the effects of hydrostatic pressure and applied electric field on the energies of electron states and binding energy of a shallow-donor impurity in two parallel coupled GaAs–$Ga_{1-x}Al_xAs$ QWW with potential W-profile. The electron wave functions in the semiconductor are obtained through an expansion in a complete set of trigonometric functions. We use the effective-mass and parabolic-band approximations within a variational procedure. Calculations are performed for symmetric and asymmetric QWW heterostructures, for two different values of the hydrostatic pressure and external electric field. In "Theoretical framework" section, we present the theory of the problem. Our results are presented and discussed in "Results and discussion", and our conclusions are given in "Conclusion" section.

Theoretical framework

Here, we are dealing with a hydrogenic donor-impurity in a GaAs–$Ga_{1-x}Al_xAs$ QWW grown along the z-axis in the presence of an applied electric field $\mathbf{F} = -F\hat{z}$, taking into account the effects of hydrostatic pressure (P). In Fig. 1 we present a pictorial view of the studied system.

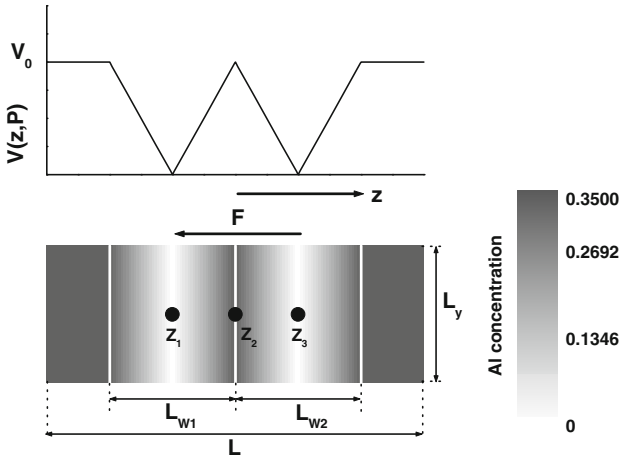

Fig. 1 Pictorial view of confining W-shaped potential profile along the z-direction with hydrostatic pressure and growth-direction applied electric field dependent for the QWW system studied here. The *filled circles* show the impurities position

Our theoretical approach uses the effective mass and parabolic-band approximations [21]; so, the Hamiltonian for the donor-impurity, in cartesian coordinates, takes the following form [22]

$$H = -\frac{\hbar^2}{2m^*(P)}\nabla^2 + V(y,z,P) - |e|Fz - \frac{e^2}{\varepsilon(P)r}, \qquad (1)$$

where $r = \sqrt{x^2 + y^2 + (z - z_i)^2}$ is the electron–impurity distance [the electron and impurity coordinates are, respectively, (x, y, z) and $(0, 0, z_i)$]. In addition, e is the the electron charge, and $m^*(P)$ and $\varepsilon(P)$ are the hydrostatic-pressure-dependent electron effective mass and static dielectric constant, respectively (for simplicity, the dielectric constant and the effective masses are considered to be the same as in GaAs throughout the whole QWW). For the GaAs electron effective mass and the static dielectric constant we have used, respectively, $\varepsilon(P) = 12.65 - 0.02\,\mathrm{kbar}^{-1}P$ and $m^*(P)/m_0 = 0.067 + 5.56 \times 10^{-4}\,\mathrm{kbar}^{-1}P$, where m_0 is the free electron mass [23, 24]. The pressure dependence on the dimensions of the heterostructure is obtained from the fractional change of the volume [24–26].

The confining potential due to the heterostructure is given by $V(y, z, P) = V(z, P) + V(y)$. The structure of $V(z, P)$ is depicted in Fig. 1, whereas $V(y) = 0$ for $|y| \leq L_y/2$ and infinite elsewhere. The shape of the $V(z, P)$ inside the wire regions is controlled by a Λ-parameter which is zero for rectangular profile and 0.5 for W-profile. We follow the model of Elabsy [1] in which the $\Gamma - X$ cross-over in the $Ga_{1-x}Al_xAs$ material—induced by the effect of hydrostatic pressure—is introduced into the model through

the pressure dependence of the height of the barrier that confines the electrons in the z-direction.

Variational techniques are a suitable tool for studying electron states—with or without hydrostatic pressure effects—in semiconducting low-dimensional systems [27–29]. In the case of our interest, we adopt the variational scheme used by Fox et al. [30] and Galbraith and Duggan [31] in order to obtain the impurity eigenfunctions for the GaAs–$Ga_{1-x}Al_xAs$ QWW. This consists of the minimizing of the energy functional

$$E = \langle \Psi(x,y,z)|H|\Psi(x,y,z)\rangle. \quad (2)$$

The trial wave function has been chosen as

$$\Psi(x,y,z) = Nf(z)\cos(\pi y/L_y)e^{-\lambda r}, \quad (3)$$

where N is a normalization constant and λ is a variational parameter. The non-correlated function $f(z)$ has been obtained via the method put forward by Xia and Fan [32], which consists of an expansion in terms of sine functions associated with the infinite barrier QW of width L. $L_{W1} \times L_y$ and $L_{W2} \times L_y$ are the transversal sections of the two coupled QWW.

Results and discussion

Figure 2 shows the energies for the first five electronic states in the QWW as a function of the Λ-confinement potential parameter with $L_{W1} = L_{W2} = 10$ nm and hydrostatic pressure $P = 25$ kbar. The height of the total transversal confinement potential is shown by a dashed line. The calculations were performed with zero electric field, Fig. 2a, and finite electric field $F = 20$ kV/cm, Fig. 2b. From these figures it can be seen that the energy increases as the Λ-parameter reaches its maximum value, 0.5 (W-profile confinement). This is caused by the extra confinement of the electron wave function due to the appearance of the central potential barrier in the middle of the double QWW. In accordance, for values of Λ smaller than 0.3, only the first three states are kept inside the QWW. BY observing Fig. 2b, it can be appreciated that, as a consequence of the applied electric field, every state is shifted to smaller energies. The states whose energies, E_n, obey the relation $E_n = \frac{\hbar}{2m^*}\frac{\pi^2}{L_y^2} + V_0 - eF\frac{L}{2}$, $n = 1, 2, 3\ldots$, are confined in the QWW with W-profile potential. In such a way, there are always at least three confined states for the whole range of Λ-parameter values. It is important to clarify that the energies, in both Fig. 2a and b, are refered to the same reference system. The energies lying over the dashed line correspond to confined states in a quantum wire of transversal section $L \times L_y$.

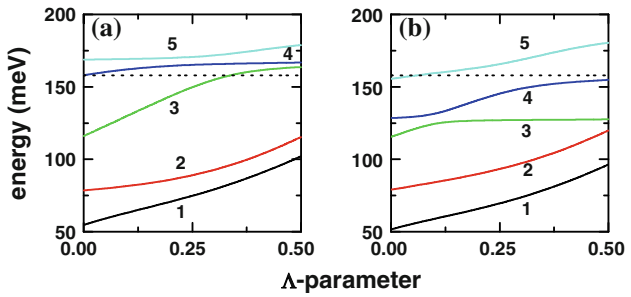

Fig. 2 The energies for the first five electronic states in a GaAs–$Ga_{0.7}Al_{0.3}As$ QWW as a function of Λ-confinement potential parameter for two different values of the in growth-direction applied electric field: **a** $F = 0$, **b** $F = 20$ kV/cm. The $L_{W1} = L_{W2}$ widths and the hydrostatic pressure were set at 10 nm and 25 kbar, respectively. The *dashed lines* represent the total transversal confinement potential

In Fig. 3, we report the results for the energies of the electronic states as a function of width of the symmetric QWW for the first five states. The calculations were performed for $P = 0$, $\Lambda = 0$, and $F = 0$, Fig. 3a; while we take $F = 20$ kV/cm for the results of Fig 3b. From these figures it can be observed that, as a general behavior, the energy of the five states decreases as the width of the QWW increases with or without applied electric field. That is, for a QWW wider than 10 nm, the first five electronic states are inside the wires regions.

Additionally, the electric field causes separation on the energy curves of the states, which is more pronounced for $L_W \geq 20$ nm. Another effect related to the influence of the electric field is the lowering of state energies. This causes a situation for which, if $L_{W1} = L_{W2} < 5$ nm, the number of confined states changes from two, when $F = 0$, to four, when $F = 20$ kV/cm. For $F = 0$ and $L_{W1} = L_{W2} \to 0$ our results reproduce the exact limit of a $Ga_{0.7}Al_{0.3}As$ QWW with infinite potential barriers and transversal section of 60 nm × 10 nm (see the full symbols compared with short

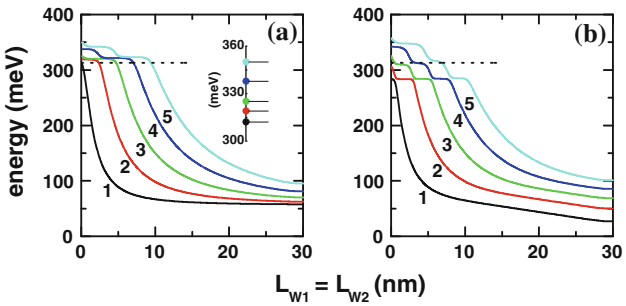

Fig. 3 The energies for the first five electronic states in a GaAs–$Ga_{0.7}Al_{0.3}As$ QWW as a function of $L_{W1} = L_{W2}$ widths corresponding to two different values of the in growth-direction applied electric field: **a** $F = 0$, **b** $F = 20$ kV/cm, for $P = 0$ and $\Lambda = 0$. The *dashed lines* represent the total transversal confinement potential. In **a** the inset shows the energies for $L_{W1} = L_{W2} = 0$ (*full symbols*) compared with the exact energy values in a 60 nm × 10 nm transversal section $Ga_{0.7}Al_{0.3}As$ QWW with infinite potential barriers (*horizontal symbols*)

horizontal symbols in the inset of Fig. 3a): $[E_n = \frac{\pi^2}{L_y^2} + \frac{n^2\pi^2}{L^2} + V_0, \quad n = 1, 2, 3\ldots$, where E_n and V_0 are given in effective Rydberg units and L_y and L are given in effective Bohr radius units]. Also for $L_{W1} = L_{W2} = 30$ nm our results correspond to the limit of a GaAs QWW with infinite potential barriers and transversal section 60 nm × 10 nm : $\left[E_n = \frac{\pi^2}{L_y^2} + \frac{n^2\pi^2}{L^2}, \quad n = 1, 2, 3\ldots\right]$. In the case of applied electric field, Fig. 3b, our results reproduce the exact limit of the Stark effect for an electron confined inside $Ga_{0.7}Al_{0.3}As$ and GaAs QW with infinite potential barriers.

The results shown in Fig. 4 correspond to the same conditions as in Fig. 3 except for the value of the hydrostatic pressure which is set at 25 kbar. In Fig. 4a, it can be seen that the effect of sole pressure is to lower the electronic state energies as well as the confinement profile height V_0. It occurs in such a way that, for instance, for a W-profile width of about 15 nm, the five electronic states lie within the QWW. This is in contrast to the pressureless case, Fig. 3a, in which the five electronic states are in the QWW, but for a width of about 10 nm. The shift of states towards lower energies is the combined effect of the increasing effective mass with pressure and the fall of the confining barrier's height. This shift to lower energies is not a linear displacement for the total confining potential and for the confined states (there is not a rigid shift of all energies). This is evident in the number of states that lie below the total potential for a certain width of the wells. For example in Fig. 3a, in the case of $L_{W1} = 5$ nm, there are three confined states; whereas in Fig. 4a and for the same width there are only two confined states. From Fig. 4b it can be seen the combined effect of the pressure and applied electric field. Again, the electric field leads to energy curves separation lowering the energies of all states. This effect is mainly observed for the two first confined states.

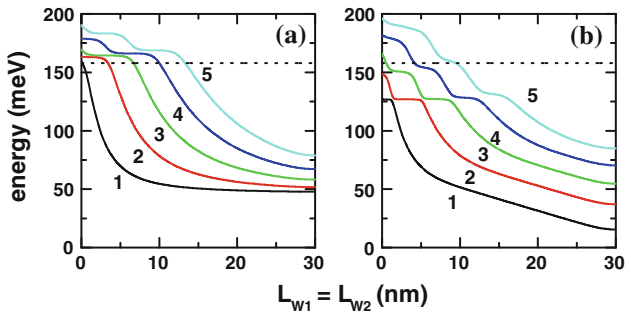

Fig. 4 The energies for the first five electronic states in a GaAs–$Ga_{0.7}Al_{0.3}As$ QWW as a function of $L_{W1} = L_{W2}$ widths for two different values of the in growth-direction applied electric field: **a** $F = 0$, **b** $F = 20$ kV/cm, for $P = 25$ kbar and $\Lambda = 0$. The *dashed lines* represent the total transversal confinement potential

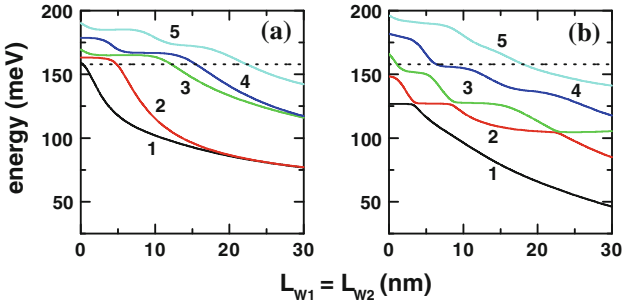

Fig. 5 The energies for the first five electronic states in a GaAs–$Ga_{0.7}Al_{0.3}As$ QWW as a function of $L_{W1} = L_{W2}$ widths for $P = 25$ kbar and $\Lambda = 0.5$. Two different values of the in growth-direction applied electric field are considered: **a** $F = 0$, **b** $F = 20$ kV/cm. The *dashed lines* represent the total transversal confinement potential

Figure 5 shows the results corresponding to the same conditions as in Fig. 4, except for the value of the Λ-parameter which is now set at 0.5. As in the case shown in Fig. 2, the effect of Λ-parameter is to increase the electronic state energies. This is clearly apparent by comparing Figs. 4a and 5a, in which we have $\Lambda = 0$ and $\Lambda = 0.5$, respectively. In the limit $L_{W1} = L_{W2} \to 0$, Figs. 4 and 5 have exactly the same energies, both for zero and 20 kV/cm values of the applied electric field. Furthermore, in Fig. 5a it can be seen that for $\Lambda = 0.5$, and in the limit of large L_W values, the energy of the consecutive states have the same value (degenerated states). This is caused by the fact that, when $L_{W1} = L_{W2} \to 30$ nm, the system becomes into two equal QWW's with a 10 nm × 15 nm transversal section, separated by a 30 nm barrier. In other words, the QWW's are not coupled due to the size of central barrier's width. In addition, Fig. 5b shows the electric field effect. The electric field breaks the degeneration of the states in the large limit of L_W. This is due to the lowering of the even states and the raising of the odd states energy implied by the orthogonality condition between them. As a result, we have the localization of the wave function in each QWW.

In Fig. 6 we show the amplitude of probability in the transversal section $(|f(z) \times \cos(\pi y/L_y)|^2)$ of a GaAs–$Ga_{0.7}Al_{0.3}As$ QWW with $L_{W1} = 10$ nm, $L_{W2} = 0$ nm. The results are for the first three non-correlated electron states considering two different values of the potential parameter: $\Lambda = 0$, left panel, and $\Lambda = 0.5$, right panel. Clearly, Fig. 6a, c corresponds to the two first even states (the wave function $f(z)$ has one and three antinodes, respectively). For the amplitude of probability, it is clear that in the left panel all figures have reflection symmetry with respect to the plane at $z = -0.5a_0^*$ and inversion symmetry with respect to the the point at $z = -0.5a_0^*$ with $y = 0$. These three states are strongly confined into the QWW region and correspond to bound states of the wire. Figure 6d, e, where

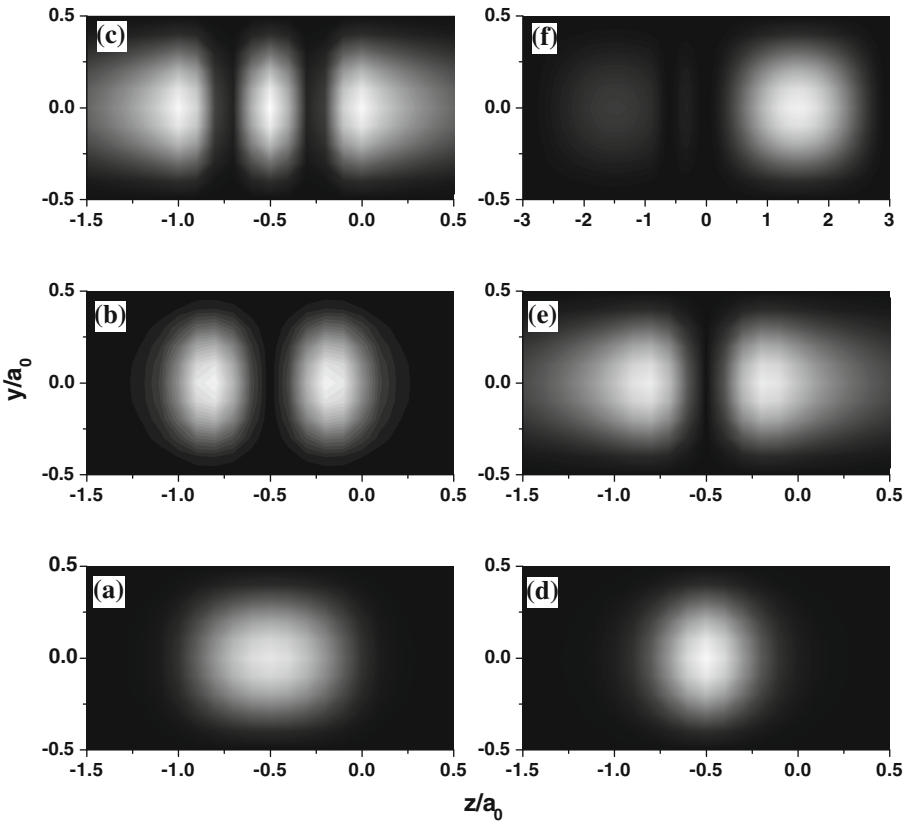

Fig. 6 Amplitude of probability in the transversal section $(|f(z) \times \cos(\pi y/L_y)|^2)$ for the first three non-correlated electron states for two different values of the potential shape parameter: $\Lambda = 0$ (**a**–**c**) and $\Lambda = 0.5$ (**d**–**f**). The L_{W1}, L_{W2} widths were set at 10 nm and 0 nm, respectively, and there was not applied electric field or hydrostatic pressure. The intensity is in arbitrary units

$\Lambda = 0.5$, corresponds to the *only* two confined states in the V-profile QWW and also they have the same symmetries observed in all figures in the left panel. The third state, Fig. 6f, loses all symmetries because it is strongly affected by the infinite barriers at $z = \pm L/2$. This state corresponds essentially to the ground state of a infinite barrier QWW with cross-section $L \times L_y$. Only a single antinode is observed which is shifted towards the barrier at $z = +L/2$; this is an applied electric field-like effect due to the V-profile potential centered at $z = -0.5a_0^*$.

For complete study of the behavior of electronic states and the binding energy of impurity, we present in Fig. 7 the amplitude of probability in the growth-direction ($|f(z)|^2$) for the first three non-correlated electron states in a GaAs–$Ga_{0.7}Al_{0.3}As$ QWW with $L_{W1} = 10$ nm, $L_{W2} = 10$ nm and $\Lambda = 0.5$ (W-profile potential). The results are for two different values of the hydrostatic pressure: $P = 0$ (Fig. 7a–c) and $P = 25$ kbar (Fig. 7d–f). The solid lines correspond to $F = 0$ whereas the dashed lines are for $F = 20$ kV/cm. For the wave functions of the even states in Fig. 7a, d, the effect of the applied electric field is to push the wave function towards the S_2 region (QWW at the right hand side). Clearly, Fig. 7c, f corresponds to extended states associated to the $L \times L_y$ QWW and in this case the applied electric field pushes the electron wave function towards the infinite barrier at $z = +L/2 = 3a_0^*$. For the odd states, Fig. 7b, e, the applied electric field confines the wave functions into the S_1 region of the W-profile QWW (QWW at left hand side). The orthonormalization of the $f(z)$ wave functions is readily apparent. The main effect of hydrostatic pressure is to spread the wave function into the whole transversal section. This is because the lowering of the confinement potential barriers as a function of P.

The asymmetric QWW case is analyzed in Fig. 8. These figures show the energies for the first five electronic states in a $Ga_{0.7}Al_{0.3}As$ QWW as a function of L_{W2}, with $L_{W1} = 10$ nm, $P = 0$ and $F = 0$. The calculations were performed for $\Lambda = 0$ and $\Lambda = 0.5$ (Fig. 8a, b, respectively). When L_{W2} goes from zero to 30 nm, the system evolves from a single QWW, S_1, with a transversal section of 10 nm × 10 nm with infinite barriers at $y = \pm L_y/2$ and finite barriers in z-direction, to a pair of wires, S_1 and S_2, with transversal sections of 10 nm × 10 nm and 10 nm × 15 nm, respectively. These two coupled wires have infinite potential barriers at $y = \pm L_y/2$ and at $z = 30$ nm, a finite potential barrier at $z = -L_{W1}$, and they are coupled by a 20 nm central potential barrier. In Fig. 8a, it is observed a diminishing in the energy of the electronic states as L_{W2} increases. As long as L_{W2} increases, the electron wave functions spread in a larger transversal section with the consequent reduction in the confinement. This behavior is in agreement with the results presented in Fig. 3a. By comparing Fig. 8a

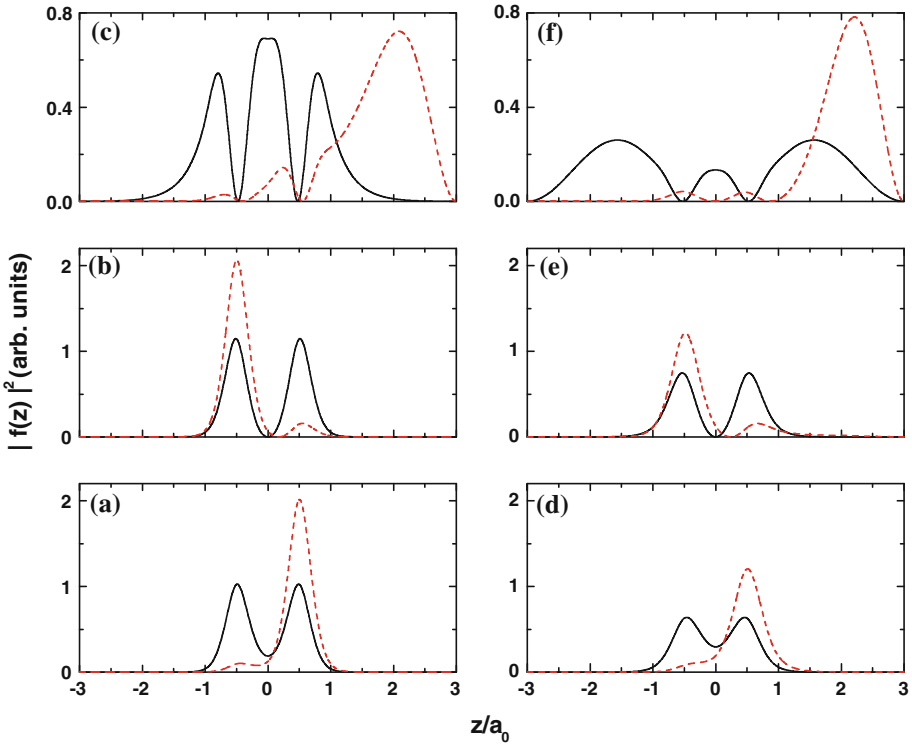

Fig. 7 Amplitude of probability in z-direction $|f(z)|^2$ for the three first electronic states in the case of a symmetric GaAs–$Ga_{0.7}Al_{0.3}As$ QWW with potential W-profile ($\Lambda = 0.5$), for different values of external hydrostatic pressure (**a–c**, for $P = 0$) and (**d–f**, for $P = 25$ kbar). The *solid* and *dashed* (black and red, online colors) lines correspond to $F = 0$ and $F = 20$ kV/cm, respectively

and b, it can be noticed that in the QWW with W-profile potential all states are shifted to higher values of energy.

In Fig. 8b, when $L_{W2} = 0$, the states with 172 meV and 304 meV correspond to the first two confined states in the S_1 region, which has a V-profile confinement potential. When $L_{W2} = 30$ nm, the states with 171 meV and 112 meV correspond to the energies of the fundamental states of the S_1 and S_2 regions, respectively. These assignments can be explained as follows: as the cross section S_1 is smaller than the cross section S_2, the fundamental state associated with the confinement in S_1 has larger energy than the fundamental state associated with the confinement in S_2. So, as L_{W2} tends to L_{W1} (symmetric system), the energy of the two fundamental states tends to be equal. This is the reason why the anti-crossing effect is presented around $L_{W2} = 10$ nm. The right panel of Fig. 8 shows the amplitude of probability in the growth direction, $|f(z)|^2$, for the first two non-correlated electron states. Fig. 8c–e correspond to different values of L_{w2} in Fig. 8b: 5, 10 and 15 nm, respectively. These values are indicated with *arrows* in Fig. 8b. The ground and the first excited states correspond to the solid and dashed lines, respectively. The inset in Fig. 8d shows the wave functions for the same states. These figures show the behavior of the two first confined states and are useful for the explanation of the anticrossing in $L_{W2} = 10$ nm. By comparing Fig. 8c and e, it can be seen that as L_{W2} increases near to the anti-crossing region, the ground state goes from the S_1 region to the S_2 region; whereas the first excited state goes from the S_2 region to the S_1 region. In Fig. 8d, it can be noticed that the amplitudes of probability are similar when the system is symmetric. In the inset the orthonormality and symmetry of these wave functions corresponding to the mentioned states (the ground state has even parity along the growth direction and the first excited states has odd parity) can be observed.

In Fig. 9, we present our results for the binding energy of a donor impurity in a GaAs–$Ga_{0.7}Al_{0.3}As$ QWW as a function of the L_{W2} size, with $L_{W1} = 10$ nm. Several values of the hydrostatic pressure and applied electric field have been considered for three special impurity positions in the transversal section of the quantum system. Calculations have been made for a W-profile QWW ($\Lambda = 0.5$). For the impurity in the S_1 region ($z_i = z_1$) (Fig. 9a), it is observed that up to $L_{W2} = 4$ nm the binding energy does not have significative changes because the dimensions of the heterostructure are small in comparison with the GaAs effective Bohr radius (~ 100 Å). Up to $L_{W2} = 10$ nm, the changes in the binding energy are not larger than 6 meV, even considering the effects of an applied electric field (curves 1 and 2). Here, the potential barriers are high enough to keep the carriers confined in the regions S_1 and S_2.

When considering pressure effects, curves 2 and 4, for $L_{W2} > 6$ nm, the binding energy drops due to the potential barriers are down more than 60% compared to its original value. In this case, the electron wave function tends to be

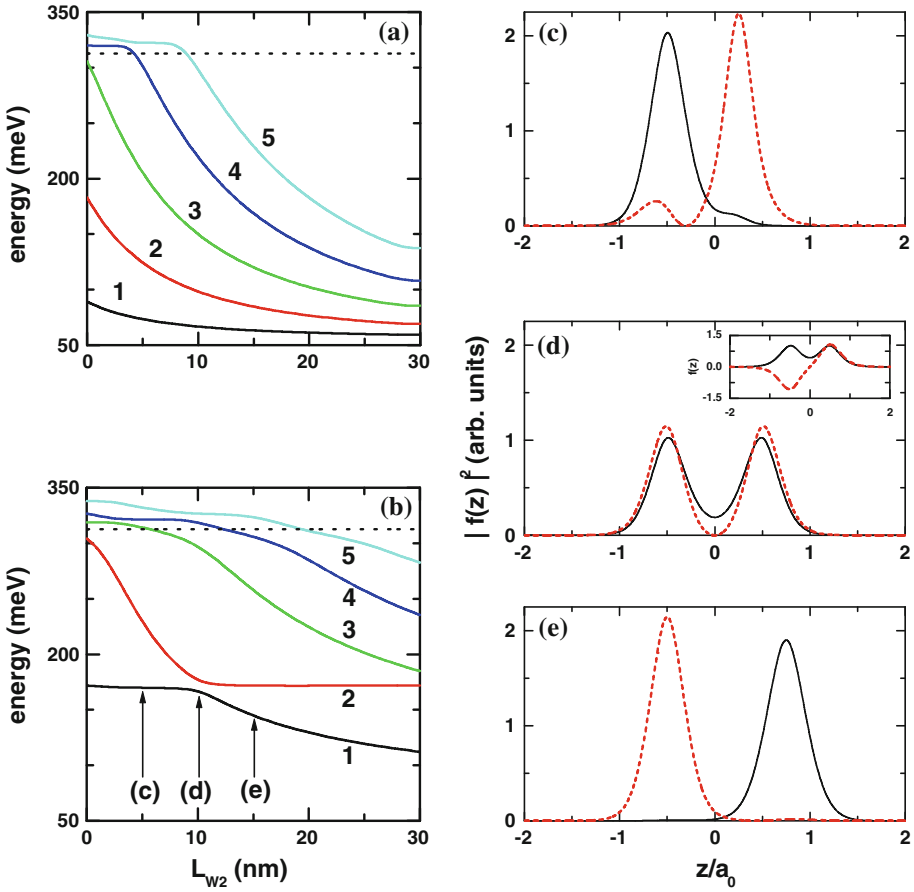

Fig. 8 *Left hand panel* The energies for the first five electronic states in a GaAs–$Ga_{0.7}Al_{0.3}As$ QWW as a function of the L_{W2} width with $L_{W1} = 10$ nm. The results correspond to $P = 0$ and $F = 0$; with $\Lambda = 0$ (**a**) and $\Lambda = 0.5$, (**b**). The *dashed lines* represent the total transversal confinement potential. *Right hand panel* The amplitude of probability in the growth-direction, $|f(z)|^2$, for the first two non-correlated electron states. **c**–**e** Correspond to different values of L_{W2}: 5, 10 and 15 nm, respectively. These values are indicated with *arrows* in **b**. The *solid lines* are for the ground state and whereas the *dashed lines* are for the first excited state. The inset in **d** shows the wave functions for the same states

localized at the midpoint of the two regions S_1 and S_2 thus increasing the electron–impurity distance and decreasing the binding energy. In this case, the effect of the hydrostatic pressure on the potential barriers is dominant over the effects of hydrostatic pressure on the GaAs dielectric constant. In Fig. 9b, for the impurity in S_2 region ($z_i = z_3$), in $L_{W2} = 0$ the binding energy corresponds to that of an impurity in the finite barrier at $z = 0$ in the region S_1, with the electron mainly located at the center of the S_1 region.

When L_{W2} takes finite values, the S_2 region—where the impurity is located—starts to appear and the binding energy begins to decrease as the electron–impurity distance grows. For $L_{W2} > 4$ nm and under the influence of electric field (curves 3 and 4) the electronic wave function is repelled to the S_2 region, with the consequent increase in the binding energy. In the case of $F = 0$ and $P = 0$, (curve 1), the growing nature of the binding energy only occurs when the system is close to the symmetric case ($L_{W2} \sim L_{W1}$), so that the probability of finding the electron in the S_1 and S_2 regions is the same. The behavior in curve 2 ($F = 0$ and $P = 25$ kbar) is similar to the observed in curve 1, but the increasing in the binding energy is smoother because of the smaller height of the potential barriers. The binding energy in $L_{W2} = 10$ nm and at $P = 25$ kbar is greater than for $P = 0$ due to the possibility that the electron wave function penetrates into the $z > L_{W2}$ region, which causes that the electron wave function becomes more symmetrical around the position of the impurity. In Fig. 9c, where the impurity is in the central barrier ($z_i = z_2$), the essentially increasing behavior of the curves 1, 2, and 3 with the increase of L_{W2} is due to the symmetrical nature, acquired by the electron wave function around the impurity. In the case of curve 4 for $L_{W2} > 6$ nm, and also for curve 2 for $L_{W2} > 8$ nm, the progressive reduction of the binding energy is because the electron wave function is located in the central region of S_2 and for it the electron–impurity distance increases with the increasing of L_{W2}, making the Coulomb interaction to decrease with the consequent drop in the binding energy.

Conclusions

Calculations of the first confined electron states and the binding energy of a shallow-donor impurity in two parallel coupled GaAs–$Ga_{1-x}Al_x$ As QWW under growth-direction applied electric field and hydrostatic pressure was performed in the effective mass and parabolic band approximations.

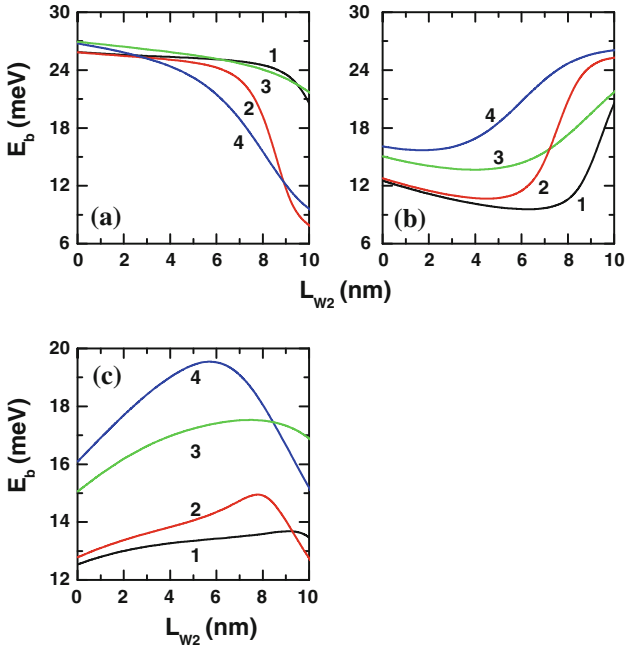

Fig. 9 Binding energies of a donor impurity in GaAs–$Ga_{0.7}Al_{0.3}As$ QWW as functions of the L_{W2} width. The lines correspond to different settings of the hydrostatic pressure and applied electric field pairs, (P, F): (0,0) (*1*), (25 kbar, 0) (*2*), (0, 20 kV/cm) (2), (25 kbar, 20 kV/cm) (*4*). In **a**, **b**, **c** the impurity position is located, respectively, at z_1, z_3, z_2 (see Fig. 1). The potential profile parameter $\Lambda = 0.5$ and $L_{W1} = 10$ nm

The theoretical results are reported for the energies of the first five electron states as a functions of the Λ-parameter (which controls the profile of the confinement potential barriers) and as a function of the size of the both QWW. We also calculated the amplitude of probability of the electronic wave function for rectangular-, V-, and W-profile for the growth-direction confinement potential ($\Lambda = 0, 0.5$). In the case of a donor impurity, we report the binding energies for the ground state and considering several positions of the impurity in the transversal section of the heterostructure. Our results can be summarized as follows: (1) for a symmetric GaAs–$Ga_{0.7}Al_{0.3}As$ QWW with W-profile potential, two uncoupled QWW are obtained when $L_{W1} = L_{W2} \geq 10$ nm; (2) the energies of the first confined electron states are increasing functions of the Λ-parameter; (3) the energies of the first confined electron states are decreasing functions of the hydrostatic pressure; (4) the binding energy of a donor impurity decreases when the system is under the effect of a hydrostatic pressure whose values here considered were taken in the regime of the $\Gamma - X$-crossover for the barrier material (25 kbar in this work)—in this case the effects of the hydrostatic pressure on the potential barriers are dominant over the effects of hydrostatic pressure on the GaAs static dielectric constant—, and finally (5) the binding energy can increases or decreases depending of the combined effects of the applied electric field and the dimensions of the transversal section of the coupled QWW.

On the other hand, it is known that the effects of polar optical phonon scattering need to be taken into account if we wish to provide a more accurate description of the electronic states for semiconducting systems based on weakly polar materials. Electron–phonon interaction is an effect that has not been considered in this work. One of its consequences is the renormalization of the confined states energies [33–35]. It should certainly affect the values of the calculated impurity binding energy. Therefore, a logical continuation of the present study is the inclusion of corrections due to such interaction. Work on this subject and also about nonlinear optical rectification in coupled QWW heterostructures are two of our future aims. Finally, we stress that to our knowledge, this is the first theoretical report about the combined effects of hydrostatic pressure and applied electric field on electron and donor-impurity states in W-profile coupled QWW. We do hope our theoretical findings stimulate future experimental researches.

Acknowledgements This research was partially supported by Dirección de Investigación de la Escuela de Ingeniería de Antioquia (cc: 1540154), the Colombian COLCIENCIAS, CODI-Universidad de Antioquia Agencies (Estrategia de Sostenibilidad Grupo de Materia Condensada-UdeA, 2009-2010), and Facultad de Ciencias Exactas y Naturales-Universidad de Antioquia (CAD-exclusive dedication project 2009-2010). The authors are grateful with the Prof. P. Aristizábal by useful discussions and suggestions.

References

1. Elabsy AM (1994) J Phys Condens Matter 6:10025
2. Duque CA, López SY, Mora-Ramos ME (2007) Phys Stat Sol B 244:1964
3. Mora-Ramos ME, López SY, Duque CA (2008) Eur Phys J B 62:257
4. Correa JD, Porras-Montenegro N, Duque CA (2006) Braz J Phys 36:387
5. Kasapoglu E, Yesilgül U, Sari H, Sökmen I (2005) Physica B 368:76
6. Barseghyan MG, Kirakosyan AA, Duque CA (2009) Phys Stat Sol B 246:626
7. Morales AL, Montes A, López SY, Duque CA, (2002) J Phys Condens Matter 14:987
8. Kasapoglu E (2008) Phys Lett A 373:140
9. Bai ZG, Liu J-J (2007) J Phys Condens Matter 19:346218
10. Kasapoglu E, Sari H, Sökmen I (2005) Physica B 362:56
11. Kasapoglu E, Sari H, Sökmen I (2003) Physica E 19:332
12. Bilekkaya A, Aktaş Ş, Okan SE, Boz FK (2008) Supperlatt Microstruct 44:96
13. Aktaş Ş, Bilekkaya A, Okan SE (2008) Physica E 40:2703
14. Niculescu EC, Radu A, Stafe M (2009) Supperlatt Microstruct 46:443
15. Vanitha A, Peter AJ (2009) Supperlatt Microstruct 46:679
16. Karabulut I, Safak H, Tomak M (2005) Solid State Commun 135:735

17. Baskoutas S, Paspalakis E, Terzis AF (2007) J Phys Condens Matter 19:395024
18. Chen B, Guo K-X, Wang R-Z, Zheng Y-V, Li B (2008) Eur Phys J B 66:227
19. Chen B, Guo K-X, Wang R-Z, Zhang Z-H (2009) Superlatt Microstruct 45:125
20. Raigoza N, Morales AL, Montes A, Porras-Montenegro N, Duque CA (2004) Phys Rev B 69:045323
21. Dzyubenko AB, Yablonskii AL (1996) Phys Rev B 53:16355
22. Zheng J-L (2008) Pysica E 40:2879
23. Li EH (2000) Physica E 5:215
24. Adachi S (1985) J Appl Phys 58:R1
25. Aspnes DE (1976) Phys Rev B 14:5331
26. Yu PY, Cardona M (1998) Fundamentals of semiconductors. Springer, Berlin
27. Mora-Ramos ME, Toledo-Solano M (2002) Phys Stat Sol B 232:142
28. Toledo-Solano M, Mora-Ramos ME (2003) Physica E 19:356
29. Mora-Ramos ME, Duque CA (2009) J Phys Conf Ser 167:012030
30. Fox AM, Miller DAB, Livescu G, Cunningham JE, Jan WY (1991) Phys Rev B 44:6231
31. Galbraith I, Duggan G (1989) Phys Rev B 40:5515
32. Xia J-B, Fan W-J (1989) Phys Rev B 40:8508
33. Mora-Ramos ME (2000) Rev Mex Fis 46:258
34. Mora-Ramos ME, Duque CA (2000) Phys Stat Sol B 220:159
35. Mora-Ramos ME (2000) In: Vlaev SJ, Gaggero-Sager LM (eds) Nova science. Huntington, New York